



SIGNIFICANCE OF MODELING, LOADING AND ANALYZING METHODOLOGIES ON THE SEISMIC RESPONSE OF CURVED BRIDGES

MR. Falamarz-Sheikhabadi⁽¹⁾, A. Zerva⁽²⁾

⁽¹⁾ Graduate Student, Department of Civil, Architectural and Environmental Engineering, Drexel University, mf585@drexel.edu

⁽²⁾ Professor, Department of Civil, Architectural and Environmental Engineering, Drexel University, zervaa@drexel.edu

Abstract

This study investigates numerically various scenarios for the seismic assessment of a tall, long-span, curved, reinforced-concrete bridge, the Mogollon Rim Viaduct, based on recent advances in bridge engineering. The bridge's geotechnical components, i.e. seat-type abutments and pile-raft foundations, its structural components, i.e. flared piers and superstructure, and soil-structure interaction are modeled in detail. The effects of P-delta, bond slip at the pier base, and pounding for both the exterior shear keys and back walls are incorporated in the finite-element model. A bin of time histories recorded during four large-magnitude earthquakes in the U.S. West Coast are selected for the seismic loading of the bridge, and conditionally simulated spatially variable strong ground motion records are generated for its non-uniform excitation. The conventional tools for nonlinear static and dynamic analyses of bridges, i.e. static pushover, incremental dynamic and response history analyses, are utilized, and their influence on the evaluation of the bridge response is examined. The effect of the multi-component, multi-support and multi-directional ground motion excitations on the bridge response is highlighted. The numerical results provide a deeper insight into the nonlinear behavior of curved reinforced-concrete bridges, and suggest practice-oriented approaches for their seismic assessment.

Keywords: Curved bridge; Soil-structure interaction; Spatially varying and uniform excitation; Static pushover analysis; Response history analysis.



1. Introduction

Bridges are an important part of the lifeline system that must remain safe to support rapid recovery after natural disasters such as typhoons, hurricanes and earthquakes. The main goal in the seismic design, assessment or retrofit of bridges is to appropriately control their global behavior using fuses and energy dissipation mechanisms in order to avoid any progressive collapse or critical local failure in the superstructure, piers and foundation system, and guarantee the bridge serviceability after the occurrence of the design earthquake. This goal can be achieved through the estimation of the most realistic relationship between the shear, axial, and flexural demand and capacity of each bridge component. In turn, this requires the suitable and sufficiently detailed finite-element modeling of the bridge, the specification of the earthquake loading, and the selection of an appropriate structural analysis method.

The seismic response of curved bridges along their transverse and longitudinal directions depends on the arch or catenary action of the superstructure, and the modeling of its flexural and axial stiffness [1]. These bridges may suffer severe damage due to rotation of their superstructure or displacement toward the outside of the curve line during strong ground motions [2]. Curvature may increase the seismic demand of interior bridge piers, and rigorous modeling approaches should be utilized to capture the complex interaction of bridge components [3]. Recent case studies indicate that curved bridges are also more vulnerable to seismic action than one may predict [4], and increasing curvature results in significant structural damage [5, 6]. However, even though bridges located in low seismic regions are generally not considered for seismic analysis or design, bridges with complex geometrical configurations including curvature may need specific attention [3].

This paper addresses the detailed numerical modeling of a tall, long-span, curved, reinforced-concrete bridge, the Mogollon Rim Viaduct, based on recent advances in bridge engineering for the determination of the lower and upper bounds of its seismic response caused by a number of realistic loading scenarios. The nonlinear three-dimensional finite-element model of the bridge is created with OpenSees [7] and incorporates the effects of all structural and geotechnical components. A series of nonlinear static and dynamic finite-element analyses are performed in order to investigate how finite-element modeling approaches, structural loading patterns, and seismic analysis methodologies may affect the seismic assessment of a curved reinforced-concrete bridge. The inelastic response of the bridge piers is examined using the damage index method. Finally, a discussion on the structural response of the Mogollon Rim Viaduct is presented, and recommendations for the safe seismic assessment of curved bridges are proposed.

2. Bridge Description and Finite-Element Model

The Mogollon Rim Viaduct, designed according to the 1983-1986 AASHTO provisions and built in 1991, is located on SR 260, which is the primary roadway between the rural towns of Payson and Heber, near the top of Mogollon Rim in Central Arizona. As shown in Fig. 1(a), it is a three-span bridge with total length of 277.3 m (with spans of 85.3 m, 103.6 m and 85.3 m) and width of 18.6 m. The bridge superstructure is a precast, prestressed concrete, continuous girder, on a curve, with an uphill grade. The bridge has wing walls on the down-slope side of the two abutments, and extensive pile foundations for the two center piers, which are located on a natural slope. The clear height of the piers is 16 m and 20.8 m. The first pier is rigidly connected to the superstructure, whereas the second, taller pier is seismically isolated from the superstructure with three elastomeric bearings. The cross section of the piers changes with increasing height and has a flared shape. The base dimensions of the piers are 2.7 m × 5.5 m and their top dimensions 2.7 m × 8.2 m as shown in Figs. 1(b) and (c). Both piers are supported on pile caps with the same size. The pile caps consist of two parts, the super cap with horizontal dimensions of 5.5 m × 5.5 m and depth of 2.3 m, and the sub cap with horizontal dimensions of 9.1 m × 9.1 m and depth of 2.3 m. The pile caps are supported on nine drilled shafts with diameter of 1.2 m as shown in Figs. 1(d) and (e). The length of the piles corresponding to the first and second abutment is 22.2 m and

Mogollon Rim Viaduct

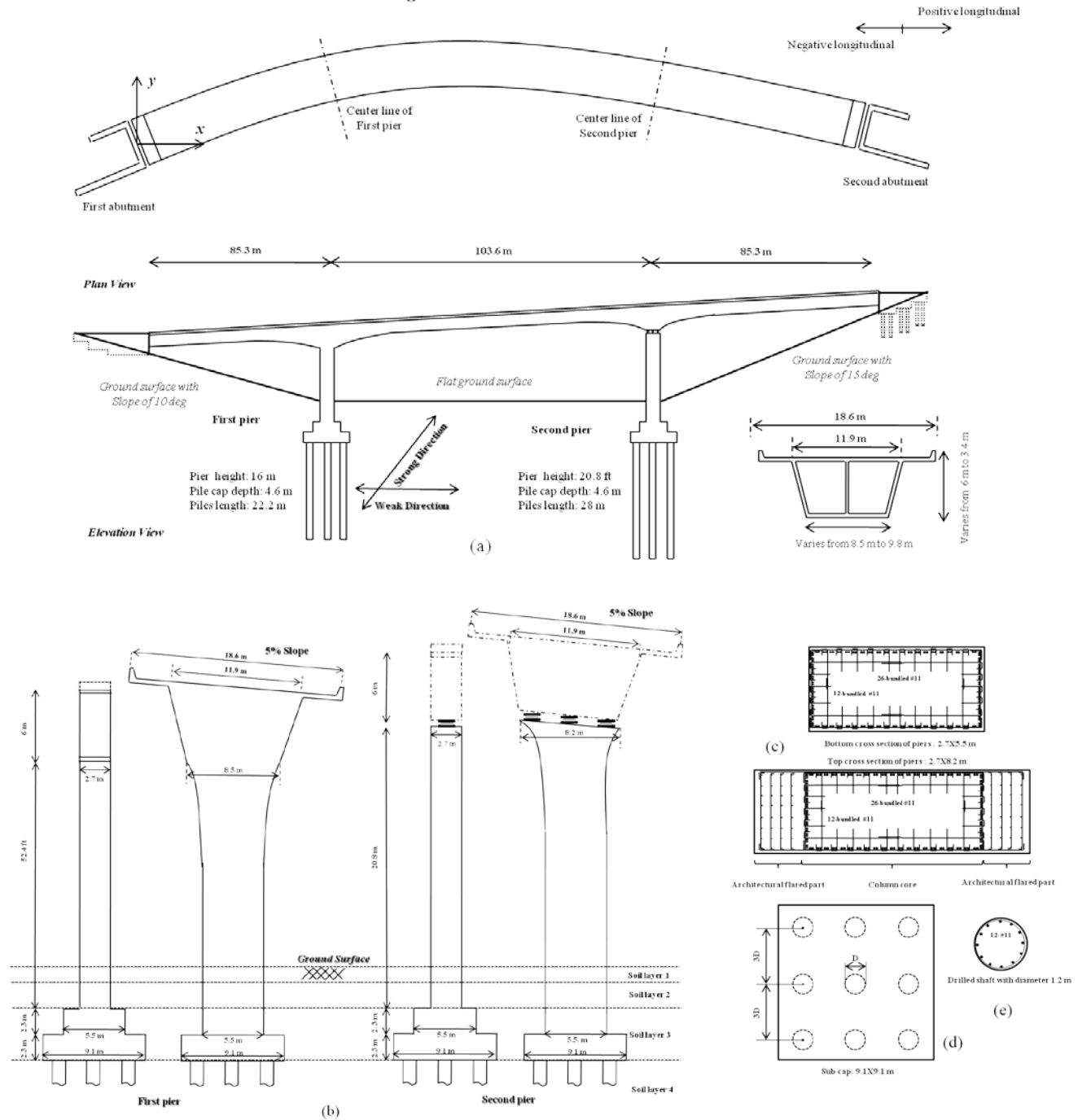


Figure 1. Structural illustration of the bridge: (a) entire bridge, (b) pier and pile foundation, (c) pier section, (d) pile cap section, and (e) pile section (scales are not the same).

28 m, respectively. The bridge has two uneven length U-shaped seat-type abutments with an asymmetric configuration of wing walls. The wing walls of each abutment are located along the longitudinal direction of the bridge and their lengths are 20.8 m and 10.8 m. The back wall is connected to the exterior shear keys and



abutment seat, and its dimensions are $13.8\text{ m} \times 3.6\text{ m} \times 0.8\text{ m}$. Both exterior shear keys have the same dimensions of $2\text{ m} \times 1.4\text{ m} \times 0.8\text{ m}$, and the abutment seat height varies from 4.1 m to 2 m along its length (19.4 m) with a constant width of 1.4 m .

The bridge superstructure is modeled using the space-frame method assuming an elastic behavior [8]. The piers and piles are modeled as three-dimensional, force-based, fiber-section, beam-column elements [9] with corotational transformation [10]. Bond slip at the pier-foundation is also considered [11]. The seat-type abutments are modeled by a combined system of nonlinear springs taking into account the possibility of the break off of the back wall in addition to the brittle failure of the exterior shear keys [12]. A Hertz contact model is considered for the effect of the superstructure-back wall pounding [13], and the elastomeric bearings are modeled using equivalent elastic-perfectly plastic springs [14]. The soil-abutment and soil-pile foundation interactions are modeled with nonlinear p-y, t-z and Q-z springs with the consideration of radiation damping [15, 16, and 17]. For the structural components, tangent-stiffness proportional damping elements are utilized assuming a minimum viscous damping ratio of 2%.

3. Analysis Framework and Seismic Loading Patterns

Two nonlinear response analysis methods are currently applied for the seismic assessment of special bridges: (1) static pushover analysis (SPA), and (2) response history analysis (RHA) [18]. The latter approach is more accurate as it considers both the cyclic response characteristics and the dynamic effects. However, it is strongly recommended [18] that the former, simpler approach is utilized for a quick assessment of failure mechanisms that may be developed and progress in the bridge due to seismic excitations (before a RHA is performed), and confirm the global response of complex bridge structures obtained from the nonlinear dynamic analysis (after the RHA has been performed). In addition to the SPA and RHA analyses, an incremental dynamic analysis (IDA) [19] is also conducted to obtain a better understanding of the nonlinear behavior of the Mogollon Rim Viaduct.

In RHA, the damage index (DI) is a useful tool to quantify the damage in structures subjected to different levels of seismic excitation. Herein, the drift damage index is used to assess the seismic damage of the bridge piers. For the piers, because multiple earthquake components are considered in the seismic excitation of the structure, the following criterion for the estimation of the damage indices due to biaxial loading along their strong ($DI_S^{Uniaxial}$) and weak ($DI_W^{Uniaxial}$) directions is used [20]:

$$DI^\lambda = DI_S^{Uniaxial} + DI_W^{Uniaxial} - \lambda \min\{DI_S^{Uniaxial}, DI_W^{Uniaxial}\} \quad (1)$$

where λ is a factor that may be assumed in the range of 0.5 to 0.85 [20, 21]. Using Eq. (1), the lower ($\lambda = 0.85$) and upper ($\lambda = 0.5$) bounds of the structural damage of the bridge piers are evaluated.

Four earthquakes that occurred in the West Coast of the United States, i.e. Loma Prieta, Northridge, San Fernando, and N. Palm Springs, are considered for the selection of the excitations. For each seismic event, accelerograms recorded mostly in the middle-field zone should be selected so that they have horizontal peak ground accelerations ($PGAs$) close to 0.2 g , which is the maximum possible acceleration in the Mogollon Rim region for a 3% probability of exceedance in 75 years based on the USGS 2014 seismic hazard map. In the present study, to preserve the nature of the ground motions, their amplitude is not scaled. Instead, considering the fundamental period of the bridge ($T_1 = 1.904\text{ sec}$), nine earthquake records with characteristics provided in Table 1 are selected so as to have a suite that meets two criteria: (1) a wide range of variations for both peak ground displacement (PGD) and peak ground velocity (PGV), and (2) horizontal $PGAs$ slightly higher than 0.2 g (considering the fact that codes provide minimum design loads). In evaluating the response of structures to multi-component earthquake excitations, the effect of the incident angle of the seismic waves should be considered in the estimation of their critical response. Various angles of incidence with respect to the principal axes of the bridge with an increment of 22.5° are considered to investigate the effect of the direction of the three-component ground excitations on its nonlinear response, i.e. each three-component earthquake record is applied



Table 1. Characteristics of nine selected strong ground motions in the radial direction.

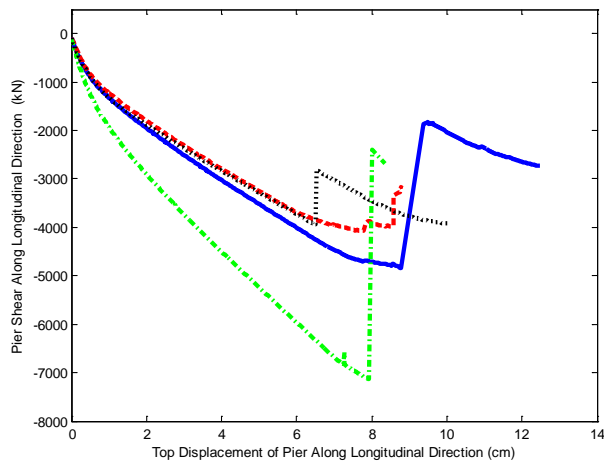
Earthquake	Loma Prieta			Northridge		San Fernando		N. Palm Springs	
	NGA0784	NGA0777	NGA0806	NGA1070	NGA1009	NGA0068	NGA0057	NGA0527	NGA0534
V_{S30} (m/sec)	306	199	267	401	391	316	450	345	370
PGD (cm)	7.4	28.6	22.8	2.9	11.2	11.7	5.0	12.2	1.1
PGV (cm/sec)	36.5	49.6	48.2	9.1	32.3	18.2	26.3	40.3	11.1
PGA (g)	0.2485	0.2271	0.2202	0.275	0.2481	0.2249	0.2731	0.2099	0.2357

at the bridge supports in sixteen different incident directions. The conditional simulation scheme proposed in Refs. [22, 23] is utilized to generate realistic spatially variable strong ground motions (SVSGMs) for the multi-support excitation of the Mogollon Rim Viaduct. The apparent wave propagation velocity for all nine seismic records used herein is assumed to be 1000 m/sec, and the coherency function utilized is based on the analysis of wave propagation through random media with the average value for the coherency drop parameter equal to 0.00025 sec/m [24].

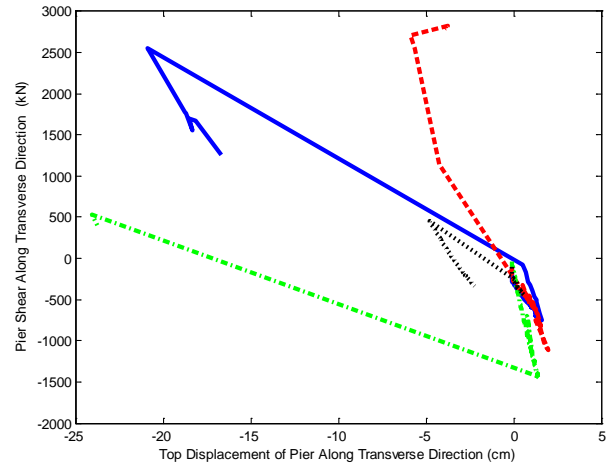
4. Bridge Response

In this section, the seismic response of the bridge under static and dynamic excitation is analyzed using SPA, RHA and IDA. The SPA is only conducted along the positive and negative directions of the global x -axis of the bridge (Fig. 1), in which the longitudinal x -direction is defined by the line connecting the centers of the two end-sections of the superstructure. This is due to the fact that the most critical seismic behavior of the bridge, due to the partial isolation of its piers, occurs along its longitudinal direction as discussed in the following. The variations of the shear force at the base of the first pier of the bridge, which is more vulnerable to seismic excitations compared to the second bridge pier, versus the deformation at its top is shown in Fig. 2. Four case scenarios are considered to investigate the effect of three important parameters in the pier modeling on the response of the bridge. “Full Model” reflects the complete finite-element model of the bridge with the consideration of bond slip (BS), architecturally flared part of the pier (Flare), and partial pier embedment (PPE). “No BS”, “No BS & No Flare”, and “No BS & No PPE” in the figure indicate the results of the models, for which these modeling parameters are not included in the finite-element analysis. The SPA is terminated when the deformation at the top of the first pier reaches 25 cm, which is the displacement corresponding to the near collapse limit state of the pier along either the transverse or the longitudinal direction of the bridge superstructure, or a major failure occurs in one of the bridge components.

For the pushover along the positive longitudinal direction of the bridge, the behavior of the first pier is analyzed in two steps, before and after contact of the back wall and the superstructure. The gap between the back wall and the superstructure is 5.08 cm. Before the contact of the superstructure with the back wall, the bridge piers are the main source of resistance against the lateral pushing forces, and, thus, the internal shear forces in the first pier increase almost linearly until the gap closes. For straight bridges, after the gap closes, the back wall becomes the main source of resistance against the lateral pushing force, and the internal shear force in the bridge piers should remain approximately constant. Hence, the participation of the back walls in resisting seismically induced loads usually leads to the decrease of the pier displacement and its ductility demand. However, this is not the case for this curved bridge and, after the gap closes, the internal forces of the first pier still increase until they suddenly drop (Fig. 2(a)) due to extensive damage (for the “No BS & No Flare” and “Full Model” models) or failure (for the “No BS” and “No BS & No PPE” models) of the exterior shear key of the first abutment. With the increase of the pushing force, the compressive axial force in the middle and right spans of the superstructure increases, more for the middle span than the right span. In order to further push the superstructure in its positive longitudinal direction, the superstructure unexpectedly undergoes a local torsional movement because of the uneven stiffness of its first and second piers. By further increasing the push along the positive longitudinal

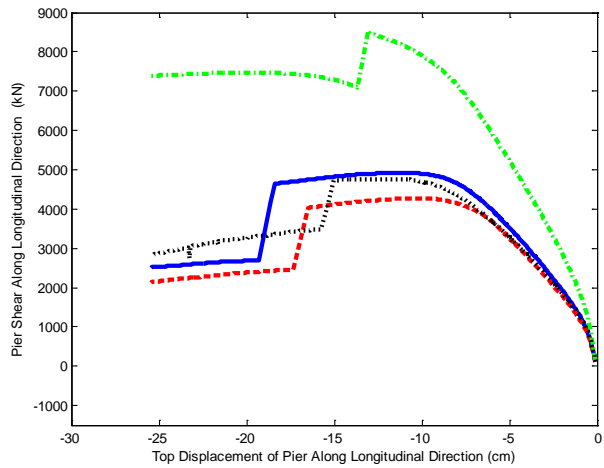


(a) Shear-displacement relationship for the first pier along the longitudinal direction

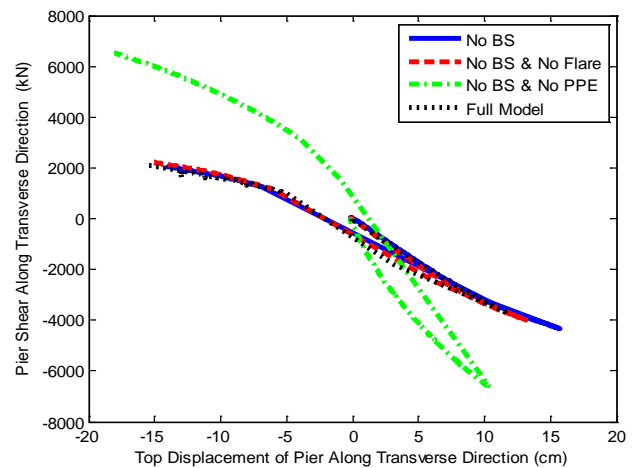


(b) Shear-displacement relationship for the first pier along the transverse direction

Pushover along the positive longitudinal direction of the bridge (Fig. 1)



(c) Shear-displacement relationship for the first pier along the longitudinal direction



(d) Shear-displacement relationship for the first pier along the transverse direction

Pushover along the negative longitudinal direction of the bridge (Fig. 1)

Figure 2. Shear force at the base of the first pier versus the top pier displacement during pushover along the positive and negative longitudinal directions of the bridge (scales are not the same).

direction of the first pier, the back wall of the second abutment acts like a very stiff obstacle, and the superstructure can only move in its transverse direction. This causes an extensive damage in the exterior shear key of the first abutment, and, subsequently, the sudden failure of the first pier. The so-called “sudden failure” is a technical term that is commonly used for shear failures, but, herein, it is used loosely to describe the rapid transition of the direction of the flexural failure of the first pier (from its longitudinal direction to the transverse one) due to the torsional movement of the superstructure. This torsional movement results in significant deformation in the transverse direction of the first pier, which is rigidly connected to the superstructure. The



maximum value of the transverse movement of the first pier (Fig. 2(b)) depends on the sudden drop of the internal shear force along its longitudinal direction (Fig. 2(a)). The different behavior of various models of the first pier in Fig. 2(b) can be attributed to the fact that it represents the failure pattern of the pier along its transverse direction due to the pushover in the positive longitudinal direction of the bridge. The required force for this torsional movement (and sudden failure) is significantly larger than the pier capacity and its occurrence may only be possible during very severe earthquakes. In Figs. 2(a), and subsequently Figs. 2(c) and (d), all pier models, except “No BS & No PPE” model behave similarly. On the other hand, significance differences can be seen in the pushover response of the first pier for the “No BS & No PPE” model in comparison to the other models. This clearly shows that the soft soil around the pier (with depth of 4.6 m) acts as a flexible support and absorbs a significant part of the lateral load applied to it. This mechanism decreases the internal shear force at the bottom of the pier and, hence, ignoring the partial pier embedment may lead to overestimation of the shear force demand in the pier.

The comparison of Figs. 2(a) and (b) with Figs. 2(c) and (d) indicates that the behavior of the bridge due to pushover in its negative longitudinal direction differs significantly from that in its positive longitudinal one. After the gap between the superstructure and the first abutment closes, the first pier controls the behavior of the superstructure, and, to accommodate the increase of its longitudinal movement, it pushes the superstructure in its transverse direction causing failure at the exterior shear key of the first abutment. The exterior shear key failure takes place when a sudden drop occurs in the internal shear force of the longitudinal direction of the first pier (Fig. 2(c)). Simultaneously, the shear force in the transverse direction of the first pier also reverses (Fig. 2(d)). The different behavior of the first pier during pushover in the negative and positive longitudinal directions is caused by the fact that, in the positive longitudinal pushover, the first pier undergoes the superstructure movement, but, in the negative longitudinal pushover, the superstructure undergoes the first pier movement, and, hence, the first pier does not fail. However, the pier effect on the superstructure, due to its significant transverse motion, is the cause of the failure of the shear keys at the first abutment for all models.

The results of the pushover response of the Mogollon Rim Viaduct clearly disagree with the concept of the partial isolation of the bridge piers to achieve symmetry as elaborated upon in the following. The effective height of the first pier of the Mogollon Rim Viaduct is approximately 4.6 m taller than its clear height (16 m), whereas the effective and clear heights of the second pier of the Mogollon Rim Viaduct are approximately the same and equal to 20.8 m. In addition, the rotational constraint at the top of the first pier is partially free in its strong direction and, therefore, its behavior is relatively close to the second pier along this direction, because both piers have approximately the same cross section, effective height and boundary conditions. In spite of the fact that the use of partial isolation to control the transverse response of the bridge may be promising, it may lead to a critical behavior of the bridge along its longitudinal direction. Based on the numerical results of this study, it appears that such a design method should not be considered appropriate for curved bridges in high seismicity areas. It is noted, however, that the Mogollon Rim Viaduct is located in a low seismicity zone.

For the dynamic analyses, the “Full Model” of the bridge pier is utilized. The maximum drifts are evaluated along the strong (d_s) and weak (d_w) directions of the first pier, which correspond, but do not coincide, with the global y - and x -directions, respectively (Fig. 1). Figs. 3(a) and (b) present these drifts for the sixteen incident angles considered for each three-component seismic record. The corresponding two biaxial damage indices DI_L^λ and DI_U^λ (Eq. 1) are presented in Figs. 3(c) and (d) to illustrate the lower ($\lambda = 0.85$) and upper ($\lambda = 0.5$) bounds of the structural damage of the pier. In Fig. 3, the record-to-record variability of the bridge response is caused by the wide variation of the peak ground velocity (PGV) of the suite of earthquakes. The most severe damage of the pier occurs for the Loma Prieta earthquake records NGA0806 and NGA0777, and the N. Palm Spring earthquake record NGA0527 (top subfigures of parts (a)-(d) in Fig. 3). The worst case scenario occurs when the bridge is subjected to the event NGA0806 with an incident angle of 22.5° , for which the lower and upper drift damage indices of the bridge pier are 0.6849 and 0.8000, respectively. This observation underlines the possibility of the formation of a significant plastic hinge at the pier base of the Mogollon Rim Viaduct due to seismic excitations with low peak ground accelerations. The ratio of the maximum value of DI_U^λ (corresponding to an incident angle of 22.5°) to its minimum value (corresponding to an incident angle of 112.5°) for the NGA0806 record as input excitation is 2.42 (0.8/0.3303). This very high ratio (242%) illustrates how the

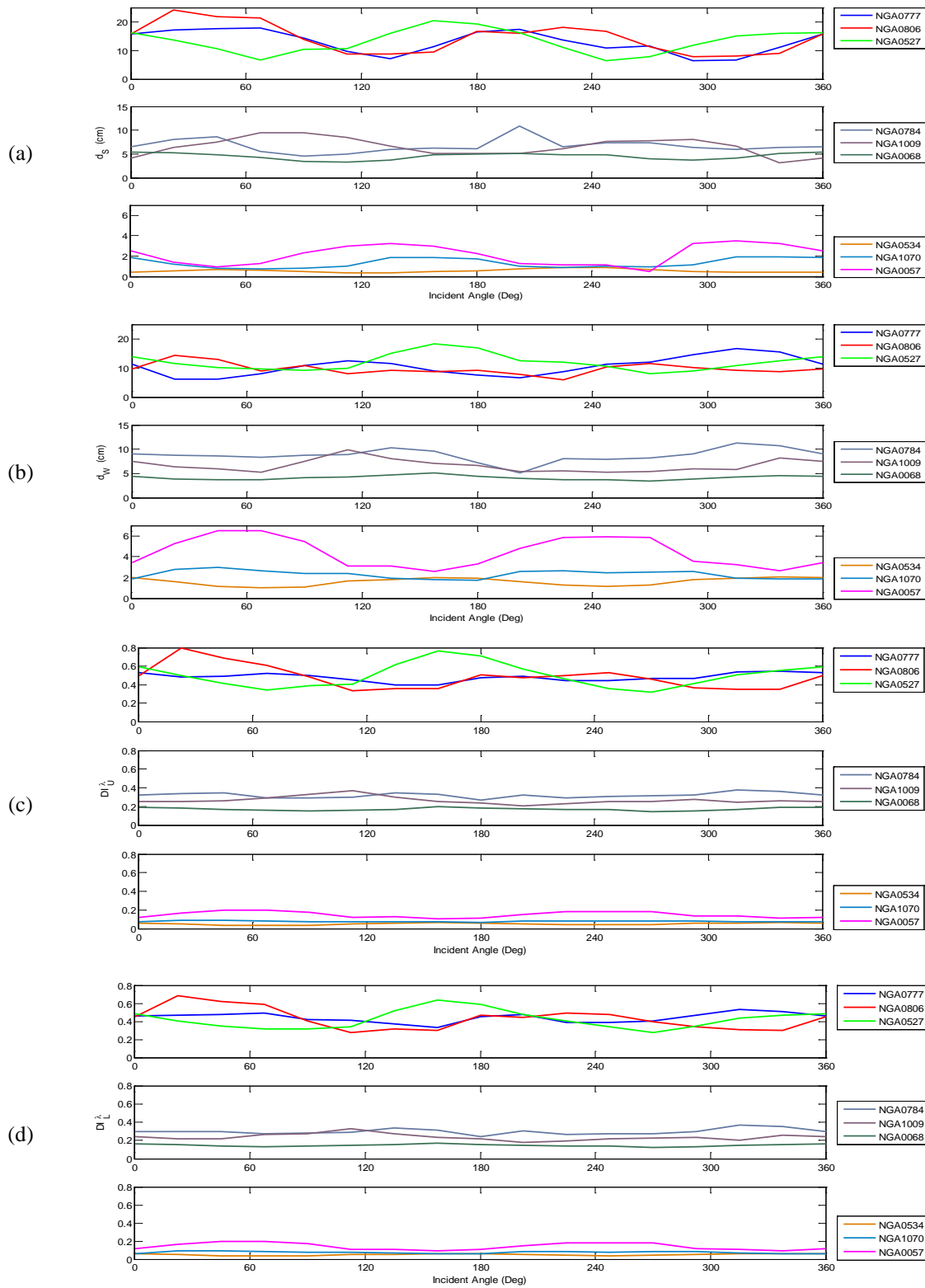
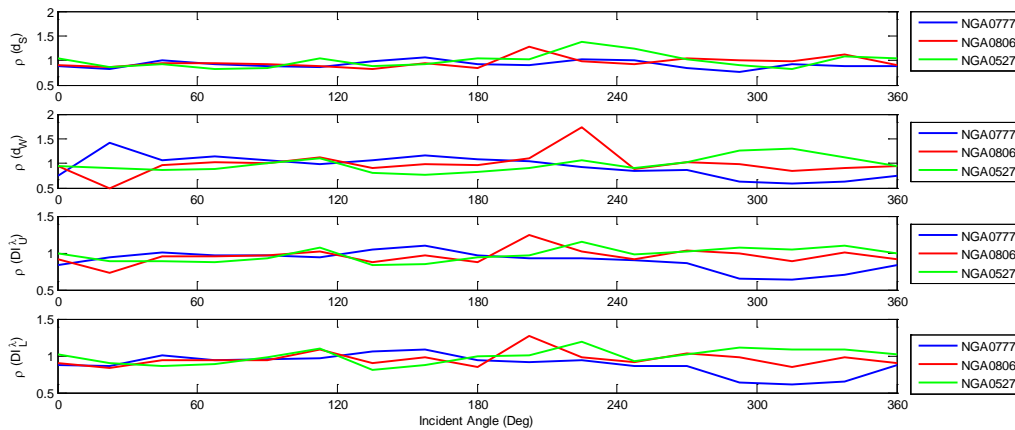


Figure 3. Variation of maximum drifts and biaxial drift damage indices of the first pier for uniform excitation versus incident angle of seismic waves: (a) pier drift along its strong direction; (b) pier drift along its weak direction; (c) upper bound of pier damage index, and (d) lower bound of pier damage index. The vertical scale of the subfigures in parts (a) and (b) are not the same.

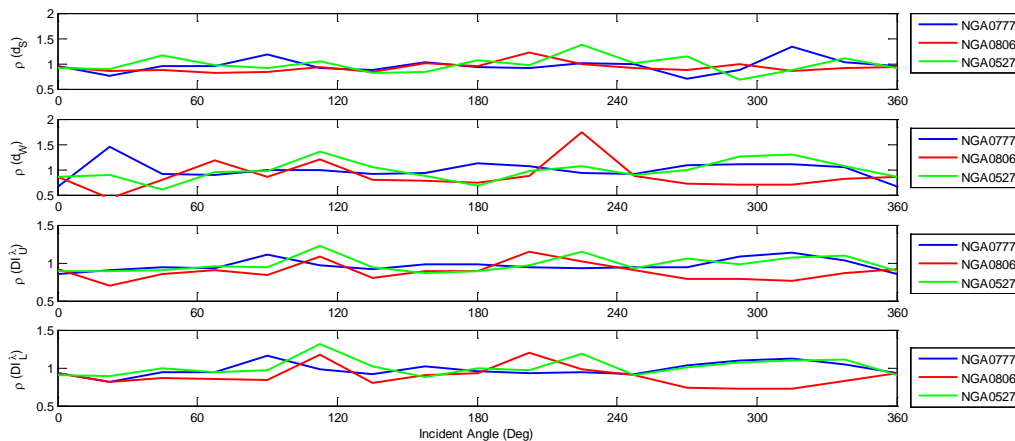


seismic response of special bridges can be significantly affected when they are subjected to a single three-component record but at different orientations with respect to the structure. Furthermore, as expected, the variation of the drift demand and the damage index of the pier is not symmetric about the incident angle of 180° due to the irregular configuration of the bridge. As an example, DI_V^{λ} of the pier caused by the NGA0806 record with incident angles of 22.5° and 337.5° is 0.8 and 0.35, respectively.

Considering that the continuous span length of the Mogollon Rim Viaduct is larger than 267 m, and that it is located on ground type C ($V_{S30}=307$ m/sec), Eurocode 8 [25] recommends that the effect of the SVSGMs should be considered in the seismic assessment of the structure. The three earthquake records that lead to the critical response of the bridge due to the uniform excitation, i.e. NGA0806, NGA0777 and NGA0527, are used as the basis for the conditional simulation. The ratio of the structural response subjected to a non-uniform excitation to its structural response subjected to the corresponding uniform excitation is denoted by ρ . Fig. 4 provides the variation of ρ for the drift and damage index of the first pier of the Mogollon Rim Viaduct for 32 incident angles. For spatially variable excitations, the bridge is subjected to 16 different incident angle orientations (Fig. 4(a)), and then the pattern is reversed, i.e. the motions that excited the first abutment now excite the second one, the motions that excited the first pier now excite the second one and so forth, for an additional 16 different incident angle orientations (Fig. 4(b)). The comparison of Figs. 4(a) and (b) suggests that



(a) First set of sixteen incident angles



(b) Second set of sixteen incident angles (reverse than those of (a))

Figure 4. Variation of ρ for the maximum drift and biaxial drift damage indices of the first pier for three time-history excitations versus the incident angle of seismic waves.



there are no significant variations in the pier response for the two patterns of application of the spatially variable ground motions. The figures further indicate that there is no clear trend when SVSGMs result in a beneficial ($\rho < 1$) or a detrimental ($\rho > 1$) effect on the pier response. The increase of the damage level of the pier in the most detrimental case due to the SVSGM effect is approximately 22%, and the decrease of the most beneficial one is approximately 39%. The results in Fig. 4 may be attributed to the fact that the fundamental frequency of the bridge is low (0.526 Hz). At such low frequencies, the spatial coherency assumes high values, i.e., the motions are still highly correlated. Furthermore, a major contribution of SVSGMs to the response of extended structures is the excitation of the pseudo-static component. However, for structures with isolated supports such as bridges, the pier foundation rotations due to the dynamic SSI effect induce pseudo-static forces, even when they are subjected to uniform excitations, that cannot be readily distinguished from the dynamic ones. On the other hand, abutments usually do not undergo significant rotations due to the dynamic SSI effect. For tall bridges built at sites with soft-to-medium soil conditions like the Mogollon Rim Viaduct, when the soil surrounding the pier foundations becomes plastic, significant pseudo-static forces are induced in the structure due to the foundation rotations, which may considerably influence the contribution of pseudo-static forces caused by the SVSGMs to the bridge response. This observation clearly underlines that ignoring the foundation flexibility may lead to an erroneous interpretation of the effect of SVSGMs on the bridge response.

Currently, there are no seismic codes providing specific guidance on how the horizontal components of an earthquake should be oriented when they are simultaneously applied to bridges and, consequently, this point is commonly ignored in conventional structural analysis methodologies. Given the results in Fig. 3, a question that may arise is how the sensitivity of the bridge response to the incident angle of seismic waves can influence the reliability of the fragility curves obtained from the conventional IDA. Fig. 5 shows the variation of the *PGV* versus the damage index of the first pier obtained from the dynamic pushover analysis of the bridge subjected to the combined action of the two horizontal components of the NGA0534 record for incident angles ranging from 0° to 337.5° . For the IDA, the NGA0534 record is utilized, because it causes the lowest damage in the first pier (Fig. 3) and, therefore, permits a significant range for the scaling effect of the accelerogram on the bridge response. The dynamic pushover analysis is terminated when the upper bound damage index of the first pier reaches 0.8 [26]. As can be seen in Fig. 5, each IDA curve corresponding to a specific incident angle shows, generally, a softening behavior with a bit of hardening. However, the pier damage is extremely sensitive to the angle of the incidence of the seismic excitation, confirming the results of Fig. 3. For example, the collapse of the first pier for incident angles of 90° and 202.5° , respectively, occurs for the scaled earthquake records with *PGV* of 157.5 cm/sec and 89 cm/sec ($157.5/89=1.77$).

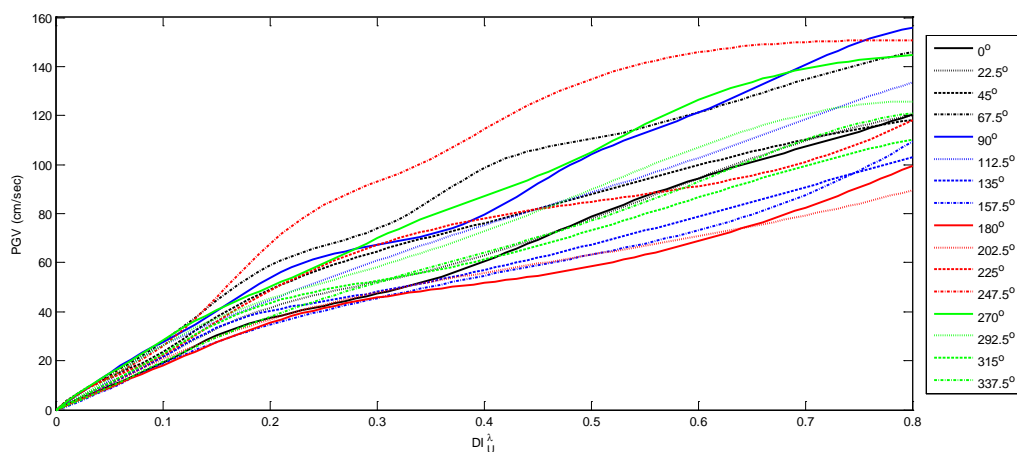


Figure 5. Variation of the damage indices of the first pier versus *PGV* obtained from the dynamic pushover analysis of the bridge subjected to the NGA0534 earthquake record with sixteen incident angles.



5. Conclusions

The present practice-oriented study assesses the seismic response of a tall, long-span, curved, reinforced-concrete bridge, the Mogollon Rim Viaduct, based on recent advances in bridge engineering. Using the SPA method that provides a clear indication of the bridge behavior, as it is easy to visualize the gradual response, the design philosophy of the partial isolation of the piers of the Mogollon Rim Viaduct for reducing the average torsional movement of the bridge due to transverse seismic loading was investigated. The numerical results indicated that this design philosophy may lead to the unexpected failure of the side piers, i.e. piers close to the abutments, because of the local torsion of the superstructure (near the abutments) of curved bridges due to longitudinal seismic loading. Therefore, caution should be applied when utilizing this design method to curved bridges. Next, using the RHA method that allows applying a realistic seismic loading, the variability of the structural response to the selection of the (uniform or nonuniform) seismic ground motions and their multi-directional incidence to the bridge was studied. It was shown that the degree of the sensitivity of the bridge response to various (uniform) input excitations and their incident angles are, respectively, more than 1000% and 240%. The consideration of the multi-support, spatially variable ground motions can further increase the sensitivity to 39%, which is not comparable to two other seismic loading factors. This observation underlines the importance of the appropriate selection of seismic loading scenarios on the seismic design and assessment of bridges. The importance of considering the effect of incident angle direction of the seismic excitations was further discussed using the IDA method that is bridging the gap between the SPA and the RHA, as it gradually increases the dynamic load. It was shown that the incident angles of the seismic excitations can significantly influence the reliability of the fragility curves obtained from the conventional IDA. For bridges located in zones with low-seismicity, bridge design codes commonly consider that linear static and dynamic analyses suffice to capture the seismic response of bridges. However, the present evaluation utilized nonlinear SPA, RHA and IDA for the seismic analysis of the Mogollon Rim Viaduct. All methodologies indicated the vulnerability of the first, shorter, rigidly-connected-to-the-superstructure pier to failure, and the necessity of using nonlinear analyses in the seismic assessment of irregular and curved bridges located in zones with low-seismicity. Based on the numerical results of this study, it can be concluded that adopting suitable structural analysis methodologies and their appropriate application for the seismic assessment are influential factors in the evaluation of the bridge response.

Acknowledgements

This study was supported in part by the U.S. National Science Foundation under Grants No. CMMI-0900179 and CMMI-1129396. Any opinions, findings, and conclusions or recommendations expressed in this material are those of the authors and do not necessarily reflect the views of the U.S. National Science Foundation.

References

- [1] Burdette NJ, Elnashai AS, (2008): Effect of asynchronous earthquake motion on complex bridges. II: Results and implications on assessment, *Journal of Bridge Engineering*, **13**, 158–165.
- [2] Japan Road Association (JRA), (2002): Specifications for Highway Bridges – Part V Seismic Design, Maruzen, Tokyo.
- [3] Wilson T, Mahmoud H, Chen S, (2014): Seismic performance of skewed and curved reinforced concrete bridges in mountainous states, *Engineering Structures*, **70**, 158-167.
- [4] HAZUS-MH [Computer software]. Washington, DC, Federal Emergency Management Agency.
- [5] AmirHormozaki E, Peckan G, Itani A, (2015): Analytical fragility functions for horizontally curved steel girder highway bridges, *Earthquake Spectra*, **31**, 2235-2254.
- [6] Pahlavan H, Zakeri B, Ghodrati Amiri G, Shaiyanfar M, (2015): Probabilistic vulnerability assessment of horizontally curved multiframe RC box-girder highway bridges, *Journal of Performance of Construction Facilities*, **12**, 1-12.



- [7] Mazzoni S, McKenna F, Scott MH, Fenves GL, et al., (2006): OpenSees Command Language Manual, University of California at Berkeley.
- [8] Hambly EC, (1991): Bridge deck behavior, Second edition, E & FN SPON.
- [9] Taucer FF, Spacone E, Filippou FC, (1991): A fiber beam-column element for seismic response analysis of reinforced concrete structures, Report No. UCB/EERC-91/17.
- [10] Crisfield MA, (1991): Nonlinear finite element analysis of solids and structures, John Wiley & Sons, **1**.
- [11] Zhao J, Sritharan S, (2007): Modeling of strain penetration effects in fiber-based analysis of reinforced concrete structures, *ACI Structural Journal*, **104**, 133-141.
- [12] Megally SH, Silva PF, Seible F, (2002): Seismic response of sacrificial shear keys in bridge abutments, Department of Structural Engineering, University of California, San Diego, Report No. SSRP-2001/23.
- [13] Muthukumar S, DesRoches R, (2006): A Hertz contact model with non-linear damping for pounding simulation, *Earthquake Engineering and Structural Dynamics*, **35**, 811-828.
- [14] Nielson BG, (2006): Analytical Fragility Curves for Highway Bridges in Moderate Seismic Zones, PhD Thesis, Georgia Institute of Technology.
- [15] Shamsabadi A, Rollins KM, Kapuskar M, (2007): Nonlinear soil-abutment-bridge structure interaction for seismic performance-based design, *Journal of Geotechnical and Geoenvironmental Engineering*, **133**, 707-720.
- [16] Boulanger RW, Curras CJ, Kutter BL, Wilson DW, Abghari A, (1999): Seismic soil-pile-structure interaction experiments and analyses, *Journal of Geotechnical and Geoenvironmental Engineering*, **125**, 750-759.
- [17] Rollins KM, Cole RT, (2006): Cyclic lateral load behavior of a pile cap and backfill, *Journal of Geotechnical and Geoenvironmental Engineering*, **132**, 1143-1153.
- [18] Kappos AJ, Saiidi MS, Aydinoglu MN, Isakovic T, (2012): Seismic design and assessment of bridges: inelastic methods of analysis and case studies, Geotechnical, Geological and Earthquake Engineering, **21**, Series Editor, Springer.
- [19] Vamvatsikos D, Cornell CA, (2002): Incremental Dynamic Analysis, *Earthquake Engineering and Structural Dynamics*, **31**, 491-514.
- [20] Qiu F, Li W, Pan P, Qian J, (2002): Experimental tests on reinforced concrete columns under biaxial quasi-static loading, *Engineering Structures*, **24**, 419-428.
- [21] Rodrigues H, Arede A, Varum H, Costa A, (2013): Damage evolution in reinforced concrete columns subjected to biaxial loading, *Bulletin of Earthquake Engineering*, **11**, 1517-1540.
- [22] Liao S, Zerva A, (2006): Physically-compliant, conditionally simulated spatially variable ground motions for performance-based design, *Earthquake Engineering and Structural Dynamics*, **35**, 891-919.
- [23] Zerva A, (2009): Spatial variation of seismic ground motions: modeling and engineering applications, Advances in engineering, CRC Press, Taylor & Francis Group.
- [24] Luco J, Wong H, (1986): Response of a rigid foundation to a spatially random ground motion, *Earthquake Engineering and Structural Dynamics*, **14**, 891-908.
- [25] CEN [Comite European de Normalisation], EUROCODE8 (2005): Design of Structures for Earthquake Resistance – Part 2: Bridges, EN 1998-2:2005, Brussels, Belgium.
- [26] Park YJ, Ang A H-S, (1985): Mechanistic seismic damage model for reinforced concrete, *Journal of Structural Engineering*, **111**, 722-739.